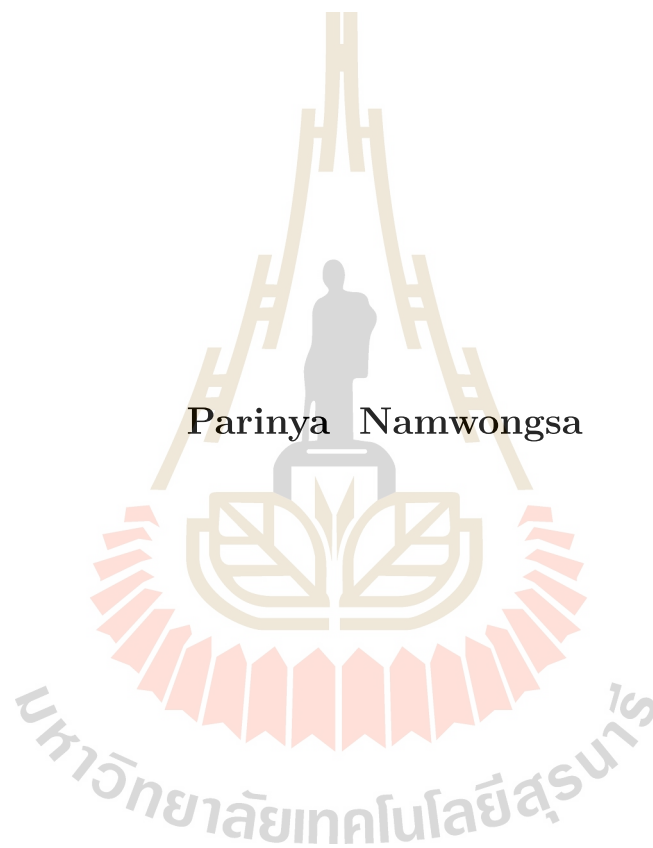


**GEOMETRY DESCRIPTION OF ALICE
INNER TRACKING SYSTEM UPGRADE**



A Thesis Submitted in Partial Fulfillment of the Requirements for the

Degree of Master of Science in Physics

Suranaree University of Technology

Academic Year 2016

รายละเอียดทางเรขาคณิตของระบบตรวจวัดชั้นใน
ที่ปรับปรุงใหม่ของหัววัดอลิซ



วิทยานิพนธ์นี้เป็นส่วนหนึ่งของการศึกษาตามหลักสูตรปริญญาวิทยาศาสตรมหาบัณฑิต
สาขาวิชาฟิสิกส์
มหาวิทยาลัยเทคโนโลยีสุรนารี
ปีการศึกษา 2559

GEOMETRY DESCRIPTION OF ALICE INNER TRACKING SYSTEM UPGRADE

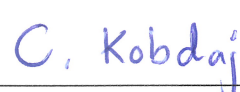
Suranaree University of Technology has approved this thesis submitted in partial fulfillment of the requirements for the Master's Degree.

Thesis Examining Committee



(Asst. Prof. Dr. Worawat Meevasana)

Chairperson



(Asst. Prof. Dr. Chinorat Kobdaj)

Member (Thesis Advisor)



(Prof. Dr. Yupeng Yan)

Member



(Asst. Prof. Dr. Ayut Limphirat)

Member



(Prof. Dr. Santi Maensiri)

Vice Rector for Academic Affairs
and Internationalisation



(Asst. Prof. Dr. Worawat Meevasana)

Dean of Institute of Science

ปริญญา นามวงศา : รายละเอียดทางเรขาคณิตของระบบตรวจวัดชั้นในที่ปรับปรุงใหม่ของ
หัววัดอลิซ (GEOMETRY DESCRIPTION OF ALICE INNER TRACKING SYSTEM
UPGRADE) อาจารย์ที่ปรึกษา : ผู้ช่วยศาสตราจารย์ ดร.ชิโนรัตน์ กอบเดช, 51 หน้า.

เครื่องเร่งอนุภาค LHC (Large Hadron Collider) จะมีการปิดเพื่อทำการปรับปรุงในปี พ.ศ.
2561-2562 โดยหลังจากการปรับปรุงครั้งนี้ เป้าหมายหนึ่งของห้องปฏิบัติการการชนของไอออน
หนัก (อลิซ, ALICE: A Large Ion Collider Experiment) คือการตรวจพบอนุภาคแลมด้าซี ซึ่งเป็น
อนุภาคแบรีออนที่เบาที่สุดที่มีชาร์มควาร์กเป็นองค์ประกอบ เนื่องจากอนุภาคนี้มีอายุสั้นและมีมวล
สูง ทำให้ต้องมีการปรับปรุงระบบตรวจวัดชั้นในขึ้นมาใหม่ โดยวิธีหนึ่งคือการลดปริมาณวัสดุที่
ใช้ทำหัววัดเพื่อลดอันตรกิริยาระหว่างอนุภาคที่เคลื่อนที่ผ่านตัวกลางในหัววัด

งานวิทยานิพนธ์ฉบับนี้มีความต้องการที่จะศึกษาปริมาณที่เรียกว่า ค่าंगวัสดุ (X/X_0 ;
material budget) ซึ่งเป็นปริมาณที่บอกถึงสัดส่วนความหนาของวัสดุที่ทำให้อนุภาคเคลื่อนที่ผ่าน
แล้วมีพลังงานลดลง $1/e$ โดยจะพิจารณาค่าंगวัสดุของหน่วยแปลงกระแสตรง (DCU: DC-to-DC
Power Supply Unit) ที่ถูกวางอยู่ภายในหัววัดและคาดว่าจะมีผลต่อความสามารถในการวัดของหัววัด
กระบวนการออกแบบและพัฒนาจะใช้ชุดซอฟต์แวร์ออลิรุท (AliRoot: ALICE Software
framework) ทำการจัดเตรียมแบบจำลองของหน่วยแปลงกระแสตรงและชนิดวัสดุที่ใช้ แล้วคำนวณ
ค่าंगวัสดุออกมาโดยใช้กระบวนการรวบรวมเส้นทางสุมในตัวกลางในช่วงมุมเอซิมัทที่ 90 องศา

ผลการคำนวณพบว่าหน่วยแปลงกระแสตรงมีค่าंगวัสดุเฉลี่ยอยู่ที่ 1.392 เพอร์เซ็นต์ ซึ่ง
ค่าเฉลี่ยที่ได้มีค่าสูงกว่าขีดจำกัดของหัววัดทั้งชั้นในและชั้นนอกที่ออกแบบไว้ในรายงานการ
ออกแบบทางเทคนิค (TDR: Technical Design Report) เนื่องจากหน่วยแปลงกระแสตรงที่ใช้ใน
การคำนวณมีลุมิเนียมเป็นองค์ประกอบหลักอยู่ถึง 69.4 เพอร์เซ็นต์ ส่งผลให้ต้องปรับเปลี่ยน
ตำแหน่งในการวางหน่วยแปลงกระแสตรงเพื่อไม่ให้กระทบความสามารถในการวัดของหัววัด

สาขาวิชาฟิสิกส์

ปีการศึกษา 2559

ลายมือชื่อนักศึกษา

ลายมือชื่ออาจารย์ที่ปรึกษา

Dr. Namwongsa

ชิโนรัตน์ กอบเดช

PARINYA NAMWONGSA : GEOMETRY DESCRIPTION OF ALICE
INNER TRACKING SYSTEM UPGRADE. THESIS ADVISOR : ASST.
PROF. CHINORAT KOBDAJ, Ph.D. 51 PP.

RADIATION LENGTH/SIMULATION/ALIROOT/INNER TRACKING
SYSTEM UPGRADE

The Large Hadron Collider (LHC) will be shut down for the upgrade in 2018-2019. After the upgrade, one of the goals of A Large Ion Collider Experiment (ALICE) is to detect the lightest charmed baryon Λ_C , which possesses the short lifetime and the high rest mass. Hence, the upgrade of the Inner Tracking System (ITS) is required. One of the ways is to reduce the material of the detector in order to decrease the effect of particle-matter interactions.

This thesis aims to study the property called material budget X/X_0 , the thickness ratio of a particle passing through the matter with its energy reduced by $1/e$, of DC-to-DC Power Supply Unit (DCU) situated inside the sensitive region. These DCUs are expected to affect the detection ability. ALICE software framework (AliRoot) is used to implement the geometry and material description of DCUs in design and development. X/X_0 is calculated by using the track-contribution approach inside the medium in 90 azimuthal angles.

The result has shown the mean material budget of DCUs is 1.392 %. It is much higher than the limit of the values of inner and outer barrels in the Technical Design Report (TDR). This high value is obtained from aluminum, which contributed 69.4 % of all materials. Therefore, these DCUs has been relocated in order to prevent their effect on the detection ability of new ITS.

School of Physics

Academic Year 2016

Student's Signature

Advisor's Signature

P. Namwongsa.

C. Kobdaj

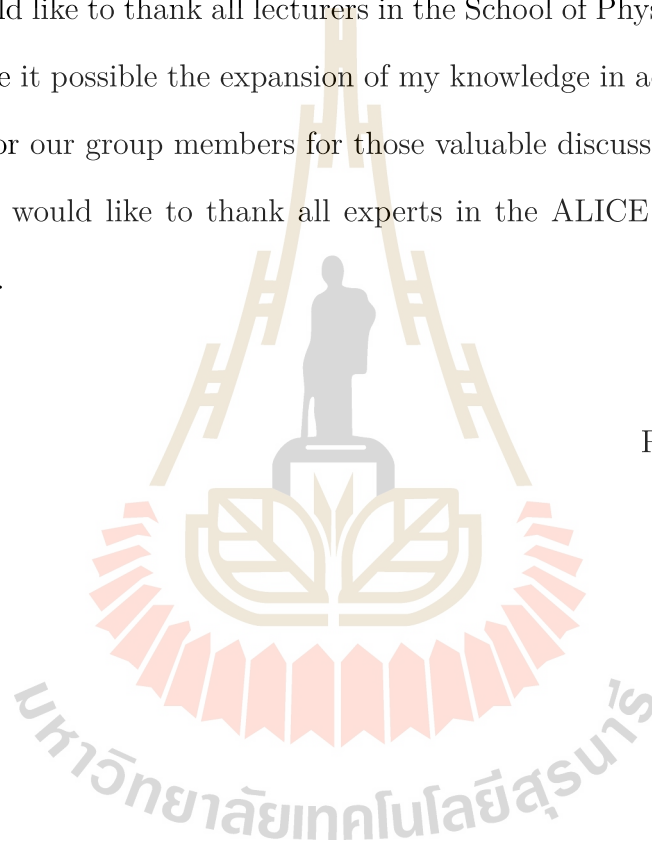
ACKNOWLEDGEMENTS

I would like to express my gratitude to Asst. Prof. Dr. Chinorat Kobdaj, my thesis advisor, for his constant support and assistance throughout the study.

I would like to thank all lecturers in the School of Physics, who have taught me and made it possible the expansion of my knowledge in academic years. Many thanks are for our group members for those valuable discussions and suggestions.

I also would like to thank all experts in the ALICE collaboration I have worked with.

Parinya Namwongsa



CONTENTS

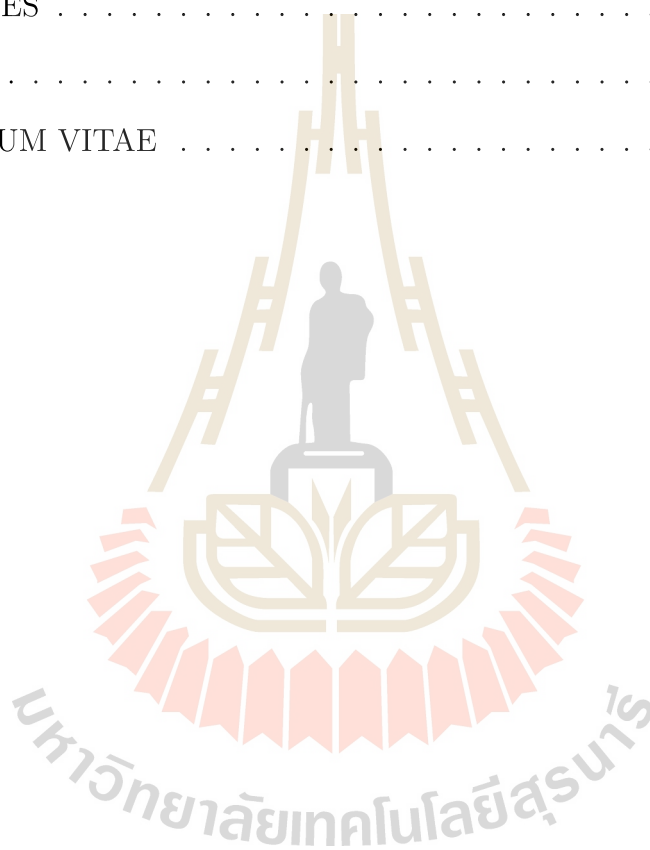
	Page
ABSTRACT IN THAI	I
ABSTRACT IN ENGLISH	II
ACKNOWLEDGEMENTS	III
CONTENTS	IV
LIST OF TABLES	VII
LIST OF FIGURES	VIII
LIST OF ABBREVIATIONS	XI
CHAPTER	
I INTRODUCTION	1
II A LARGE ION COLLIDER EXPERIMENT AT LHC	3
2.1 ALICE Detectors	3
2.1.1 Central Detectors	3
2.1.2 Forward Detectors	5
2.1.3 Muon Spectrometer	5
2.1.4 Peripheral Detectors	5
2.2 Detector Upgrades	5
2.3 Physics at ALICE Upgrade	6
2.4 Computing Framework	8
2.4.1 ALICE off-line framework: AliRoot	8
2.4.2 ALICE-FAIR on-line framework: ALFA	11
2.4.3 ALICE on-line and off-line framework: O ²	11

CONTENTS (Continued)

	Page
III INTERACTION OF PARTICLES WITH MATTER	15
3.1 Radiation Length: X_0	16
3.2 Energy Loss by Ionization	17
3.3 Energy Loss by Bremsstrahlung and Pair Production	19
3.4 Energy Loss by Electromagnetic Cascade	20
3.5 Angle Deflection by Multiple Coulomb Scattering	21
3.6 Material Budget: X/X_0	22
IV DETECTOR GEOMETRY AND IMPLEMENTATION	25
4.1 Inner Tracking System (ITS)	25
4.2 ITS Upgrade (ITSU)	26
4.3 ITSU with DC/DC Converter Unit (DCU)	27
4.3.1 Material Description	30
4.3.2 Implemented Geometry	31
V RESULT AND CONCLUSION	33
5.1 X/X_0 Contribution	33
5.1.1 Contribution to a Track	34
5.1.2 Contribution to a Scenario	34
5.1.3 Contribution to a Region	35
5.2 Calculation Processes	36
5.2.1 Earlier Processes with Stave	36
5.2.2 Modified Processes with DCU	37
5.2.3 Consistency of The Modified Processes	38

CONTENTS (Continued)

	Page
5.3 Results	38
5.4 Conclusion	39
REFERENCES	41
APPENDIX	48
CURRICULUM VITAE	51



LIST OF TABLES

Table		Page
2.1	Summary of physics ability in term of the minimum accessible transverse momentum p_T and of statistical uncertainties for an integrated luminosity 10 nb^{-1} with minimum-bias data collection. v_2 is a value of elliptic flow measurements. (Abelev et al., 2014b) . . .	9
2.2	Expected production yields in minimum-bias and 1-10 % central Pb-Pb at $\sqrt{S_{NN}} = 5.5 \text{ TeV}$. (Abelev et al., 2014b)	10
3.1	The values of L_{rad} and L'_{rad} for calculating the radiation length (Tsai, 1974).	16
3.2	List of estimated contributions of the inner layer stave to the material budget. Note that D is the thickness of the component. (Abelev et al., 2014a)	24
5.1	The build level scenarios for material budget calculation.	34
A.1	The material contribution of DCM PCB.	48
A.2	The material contribution of DCM SHIELD.	49
A.3	The material contribution of DCM PASSIVE.	50

LIST OF FIGURES

Figure		Page
2.1	The schematic layout of the ALICE experiment. The 18 different detector systems are labeled in the figure. The detectors of a central part are located inside a solenoid magnet (big red color). The muon spectrometer is placed as a forward part. The insert top right is visualization closed to the interaction region. (Schukraft, 2012)	4
2.2	The Standard Model of elementary particles with quarks, leptons and gauge bosons. (wikipedia.org)	7
2.3	The schematic layout of the ALICE software framework: AliRoot. (Cortese et al., 2005)	13
2.4	The organization of the on-line, simulation and reconstruction (off-line) processes. (Cortese et al., 2005)	13
2.5	The organization of multiple threads run in parallel independently in ALFA nodes. (Al-Turany et al., 2014)	14
2.6	The data flow diagram for on-line reconstruction and calibration of the O ² . (Adam et al., 2015)	14
3.1	The examples of mean ionization loss rate in different material as a function of $\beta\gamma = p/Mc$ for muons, pions and protons, in bubble chamber. (Patrignani et al., 2016)	17

LIST OF FIGURES (Continued)

Figure	Page
3.2 The mass stopping power for positive muons in copper against $\beta\gamma = p/Mc$. Solid curve is the total value. Vertical band is used for dividing the region of different approximation. The dotted line labeled “ μ^- ” is the Barkas effect for negative muons at low-energy of Bethe region. (Patrignani et al., 2016)	18
3.3 An EGS4 simulation of a 30 GeV electron-induced cascade in iron shown the differences between the shape of photons (square) and electrons (circle). The histogram shows fraction energy deposition per ration length, and the curve is a gamma function fit to the distribution. (Patrignani et al., 2016)	21
3.4 The layout of multiple Coulomb scattering shown the particle will be deflected in a small angle θ_{plane} in the plane of the figure. (Patrignani et al., 2016)	22
4.1 The ITS layout (Aamodt et al., 2008).	25
4.2 ALICE ITS upgrade design layout (Musa, 2012).	26
4.3 The layout of the new ITS barrels. Both Inner Barrel (IB) and Outer Barrel (OB). The visualization shown the half barrel for each types. (Aamodt et al., 2008)	27
4.4 The IB layout of the new ITS candidate model with DCU. (Corrado, 3D(STP): 20151110_IB)	28
4.5 The DCU layout for each unit of ITS Stave. (Corrado, 3D(STP): 20151110_IB)	29

LIST OF FIGURES (Continued)

Figure		Page
4.6	The layout of three DCM geometrical: PCB (grey plate), SHIELD (big pink box) and PASSIVE (small pink box) mixtures. (Corrado, 3D(STP): 20151110_IB)	30
4.7	The layout of heat exchange plate and fluid pipes of a DCU. (Corrado, 3D(STP): 20151110_IB)	31
4.8	The layout of connectors at the tail of DCU. (Corrado, 3D(STP): 20151110_IB)	31
4.9	The layout of three layers of DCU in different detector coordinates. (Corrado, 3D(STP): 20151110_IB)	32
4.10	The geometry of the ITSU IBSB with DCU which is already committed into AliRoot framework.	32
5.1	The result of material contribution of the ITSU stave L0 (first layer) is calculated from the earlier calculation processes. The horizontal line is the mean value.	37
5.2	The material contribution of the ITSU IBSB DCU L1 with $\phi = 0 - 90^\circ$ is calculated from the modified calculation processes. The horizontal line is the mean value.	39

LIST OF ABBREVIATIONS

CERN	The European Organization for Nuclear Research
ALICE	A Large Ion Collider Experiment
QGP	Quark-Gluon Plasma
ITS	Inner Tracking System
ITSU	Inner Tracking System Upgrade
IB	Inner Barrel
OB	Outer Barrel
DB	Detector Barrel
SB	Service Barrel
DCU	DC/DC Power Supply Unit
DCM	DC/DC Power Supply Module
SPD	Silicon Pixel Detector
SDD	Silicon Drift Detector
SSD	Silicon micro-Strip Detector
PCA	Point to Closest Approach
PID	Particle Identification

CHAPTER I

INTRODUCTION

ALICE (A Large Ion Collider Experiment) is one of the experiments at CERN. It is located at Point 2 (P2), where the collision of particles from Large Hadron Collider (LHC) occur (Aamodt et al., 2008). The main purpose of ALICE is to study the physics of Quark-Gluon Plasma (QGP). The QGP is a state of strongly interacting matter that quarks and gluons are not confined together in any bound states (Satz, 2011). They can freely move in a very short time at extremely high temperature and/or density. It is believed that this plasma state used to occur in a few milliseconds after the big bang. When this plasma expands, the temperature of the medium decreases. Then, quarks and gluons will combine together and form some kind of hadronic particles. This process is known as hadronization. One hadron that we are interested is Λ_C (Belikov, 2011) because it is the smallest baryon with charm quark. Currently, at LHC Run 1, it never been detected.

One of the requirements in ALICE Inner Tracking System (ITS) upgrade for the LHC Run 3 is to detect the Λ_C particles from the heavy-ion collision at ALICE (Abelev et al., 2014b) and (Musa, 2012). Since Λ_C particles possess high rest mass and easily lose their energy when traveling through the medium, therefore, it is important to keep the materials used in the detectors at the minimum. This requirement in particle detector is known as *material budget*.

Reducing of the material budget of the ITS detector is one important key to improve tracking performance properties. First, without the geometry description,

the material budget calculation is the summing overall material budget of each component. The result shows the average value of material budget but it cannot tell the specific value in each region of detectors. At this point, if we want to get the detailed information about material budgets, we have to include the geometry description in our calculation.

In high energy physics communities especially at CERN, we use ROOT data format, or “.root”. It turns out that in our work AliROOT is the most suitable and efficient way to create geometry “.root” files. AliROOT framework has been developed by the ALICE collaboration for ALICE detector. It can import “.root” data format and calculate the material budget. The result show detailed information which is useful in the development process of ALICE ITS upgrade.

In this thesis we give an overview of ALICE in Chapter II together with its up upgrade plan. The material budget contribution, in term of the radiation length, is given at the end of Chapter III. Chapter IV explains the implemented detector geometry for one of the candidate models of the new ITS. Chapter V provides the material budget calculation and their results.

CHAPTER II

A LARGE ION COLLIDER EXPERIMENT AT LHC

2.1 ALICE Detectors

ALICE (A Large Ion Collider Experiment) is a heavy-ion detector at the CERN LHC. It is designed to study the physics of Quark-Gluon Plasma (QGP) through the collision of heavy nuclei (Pb-Pb), proton-nucleus (p-Pb) and proton-proton (p-p).

The current ALICE consists of 18 different detector systems (Aamodt et al., 2008). It is 26 m long, 16 m high, and 16 meters wide with a total weight of approximately 10,000 tons. It is located in the cavern about 50 m below ground near St-Genis-Pouilly in France. Its schematic layout is shown in Figure 2.1.

2.1.1 Central Detectors

The most central detectors are embedded in a magnetic field of 0.5 T inside a big solenoid magnet, in order to determine the charged and momentum of particles through track bending.

There are three barrel tracking detectors, the Inner Tracking System (ITS), the Time Projection Chamber (TPC) and the Transition Radiation Detector (TRD) covering the pseudorapidity region from 1 to -1, 45° to 135° of beam's direction at the interaction point. The ITS is divided into three sub-detectors which are the Silicon Pixel Detector (SPD), the Silicon Drift Detector (SDD) and

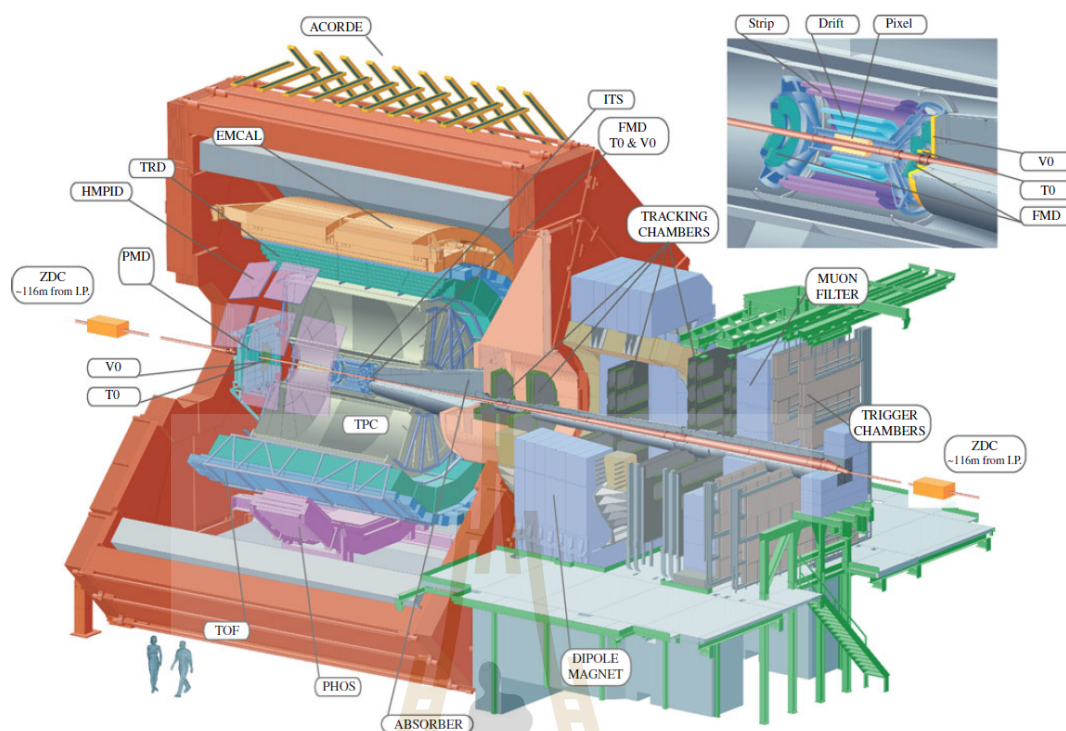


Figure 2.1 The schematic layout of the ALICE experiment. The 18 different detector systems are labeled in the figure. The detectors of a central part are located inside a solenoid magnet (big red color). The muon spectrometer is placed as a forward part. The insert top right is visualization closed to the interaction region. (Schukraft, 2012) the Silicon micro-Strip Detector (SSD).

The Time Of Flight (TOF) detector, located next to the TRD, measures the high-precision particle's velocity. The very fast particles can be detected via Cherenkov effect in the High Momentum Particle Identification Detector (HMPID).

All particle's energies except muons and neutrinos are measured inside the Photon Spectrometer (PHOS) and the Electro-Magnetic Calorimeter (EMCal). The ALICE Cosmic Rays Detector (ARCORDE) at the top of the solenoid magnet is used for detecting the high energy atmospheric muons from cosmic ray showers.

2.1.2 Forward Detectors

The multiplicity of charged particles and photons in the forward regions are detected by the Forward Multiplicity Detector (FMD) and the Photon Multiplicity Detector (PMD), respectively. The centrality of the collision can be estimated by the V0 Detector. The T0 Detector performs as a trigger and luminosity detector in order to get the reference signal for the Time-of-Flight detectors in the particle identification process.

2.1.3 Muon Spectrometer

The forward Muon Spectrometer, with its dipole magnet, and the Muon Trigger are located next to the solenoid magnet. They are used for studying the heavy quarkonia, such as J/ψ or ψ' , via their muon's decay channels. These detectors cover the forward pseudorapidity region of 2.5 to 4, 2° to 9° of beam's direction at the interaction point.

2.1.4 Peripheral Detectors

Apart from that detector parts, the Zero Degree Calorimeter (ZDC) is placed about 116 meters far from the interaction point in order to estimate the overlapping region of the two colliding nuclei.

2.2 Detector Upgrades

The next ALICE detector upgrade will operate at the second long shutdown (LS2, 2018-2019). The main goals are: 1) probe the collision with read-out rate at 50 kHz for Pb-Pb and 100 kHz for p-p and p-Pb interactions in minimum bias trigger mode, and 2) improving the tracking precision.

For ITS, the upgrade consists of new seven-layers detectors with the smaller diameter corresponding to the new beam pipe, the service barrels for installation scheme, the reduction of the material budget by using Monolithic Active Pixels Sensors (MAPS), the optimization of peripheral devices, high granularity pixel sensors and the continuous read-out mode. These improvements allow measuring the charmed and beauty, mesons and baryons at low transverse momentum region close to zero.

For TPC, the existing Multi-Wire Proportional read-out Chambers (MWPC) will be replaced by the Gas Electron Multiplier (GEM) read-out chambers. The operation mode is also changed from gated mode to continuous and triggerless modes. These improvements are for better read-out rate.

For Muon Spectrometer, the new Muon Forward Tracker (MFT) detector will be included to enable the secondary vertex reconstruction for muon tracks. It allows a very low transverse momentum measurement for quarkonia (J/ψ , ψ') and low-mass dimuon.

The remaining detectors also go general and electronic upgrades to improve the increasing data rate requirement (Cortese et al., 2005).

2.3 Physics at ALICE Upgrade

There are several aspects of physics at ALICE in order to study the QGP (Satz, 2011) properties from the collisions such as particle multiplicity, particle spectra, strangeness production, baryon-number transfer in rapidity, particle correlations, heavy-flavor production, jet studies, photon production, diffractive physics and double-parton collisions which details are given in Physics Performance Report I (Cortese et al., 2004) and II (Alessandro et al., 2006).

For ALICE upgrade, the physics motivations are outlined in three main

parts: heavy-flavor production, production of quarkonia and low-mass dileptons. The most geometry upgrade will be implemented in the ITS which is dominated the physics capability for possible observables (Abelev et al., 2014c). One of the main purposes of the new ITS is to detect the charm quark through Λ_C^+ particle from heavy-ion collision.

In the Standard Model of elementary particles, shown in Figure 2.2, the six flavors of quarks are divided into light and heavy quarks. Light quarks consist of Up (u), Down (d) and Strange (s). Heavy quarks consist of Charm (c), Bottom (b) and Top (t).

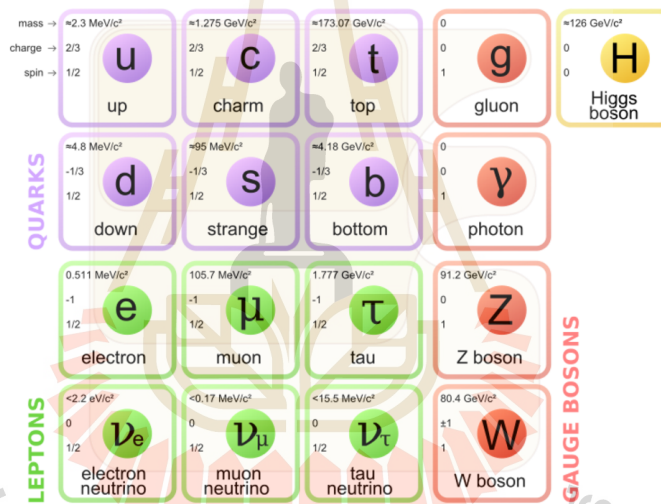


Figure 2.2 The Standard Model of elementary particles with quarks, leptons and gauge bosons. (wikipedia.org)

Light quarks with masses in a range of 1-10 MeV were detected in ALICE but not the heavy one. Charm quark is the lightest heavy quark with the mass of approximately 1.275 GeV and could be detected through charmed lambda baryon, such as Λ_C^+ , which is the lightest boundary state of baryon contained charm quark. Since the decay length of Λ_C^+ is $60 \mu\text{m}$, it is recommended that the sensor thickness should be less than $50 \mu\text{m}$.

The physics ability of the new ITS compared to the current ITS are es-

estimated in the Table 2.1. The expected production yields for those interesting particles are obtained from the Next-to-Leading Order (NLO) perturbative Quantum Chromodynamics (pQCD) calculation. (Mangano et al., 1992). These yields are shown in Table 2.2.

2.4 Computing Framework

ALICE collects the data through the Data Acquisition (DAQ) system by triggering the selective events from TRG (the Trigger system) and the High Level Trigger (HLT) system. The detector is controlled by the real-time control systems, Detector Control System (DCS) and Experiment Control System (ECS). All of above are incorporated into the *on-line* system (Fabjan et al., 2004).

The *off-line* computing framework has been developing during the detector construction called AliRoot (Cortese et al., 2004). AliRoot is built for 1) simulation of the particle collision and its detector response for the p-p and heavy-ion interactions, 2) reconstruction and analysis for both simulations and real experiments. It has been using up to the present time, the LHC Run 2.

For the LHC Runs 3 and 4, the cost reduction for the increasing of data volume requires the on-line reconstruction and calibration processes. The new developing framework thus combined the on-line and off-line systems, namely the ALICE Online-Offline Computing System (O²).

2.4.1 ALICE off-line framework: AliRoot

AliRoot is implemented on the object-oriented architecture and based on the ROOT framework (Cortese et al., 2005). It contains all of sub-detectors's information such as geometry description, detector parameters, alignment data and calibration data. As presented in the Figure 2.3, the simulation can be performed

Table 2.1 Summary of physics ability in term of the minimum accessible transverse momentum p_T and of statistical uncertainties for an integrated luminosity 10 nb^{-1} with minimum-bias data collection. v_2 is a value of elliptic flow measurements. (Abelev et al., 2014b)

Observable	Current, 0.1 nb^{-1}		Upgrade, 10 nb^{-1}	
	p_T^{\min} (GeV/c)	statistical uncertainty	p_T^{\min} (GeV/c)	statistical uncertainty
Heavy Flavour				
D meson R_{AA}	1	10 %	0	0.3 %
D_s meson R_{AA}	4	15 %	< 2	3 %
D meson from B R_{AA}	3	30 %	2	1 %
J/ψ from B R_{AA}	1.5	15 %	1	5 %
B^+ yield	not accessible		2	10 %
$\Lambda_C R_{AA}$	not accessible		2	15 %
Λ_C/D^0 ratio	not accessible		2	15 %
Λ_B yield	not accessible		7	20 %
D meson v_2 ($v_2 = 0.2$)	1	10 %	0	0.2 %
D_s meson v_2 ($v_2 = 0.2$)	not accessible		< 2	8 %
D from B v_2 ($v_2 = 0.05$)	not accessible		2	8 %
J/ψ from B v_2 ($v_2 = 0.05$)	not accessible		1	60 %
$\Lambda_C v_2$ ($v_2 = 0.15$)	not accessible		3	20 %
Di-electrons				
Temperature (intermediate mass)	not accessible			10 %
Elliptic flow ($v_2 = 0.1$)	not accessible			10 %
Low-mass spectral function	not accessible		0.3	20 %
Hypernuclei				
${}^3_\Lambda\text{H}$ yield	2	18 %	2	1.7 %

Table 2.2 Expected production yields in minimum-bias and 1-10 % central Pb-Pb at $\sqrt{S_{NN}} = 5.5$ TeV. (Abelev et al., 2014b)

Part.	Yield	$dN/dy _{y=0}$	$ct(\mu\text{m})$	decay channel	branching ratio
D^0	23, 110	2.3, 11	≈ 120	$K^-\pi^+$	3.8 %
D^{*+}	9, 44	0.9, 4.4	≈ 0	$D^0\pi^+$	67.7 %
D_S^+	4.3, 20	0.4, 2.0	≈ 150	$\phi(\rightarrow K^+K^-)\pi^+$	4.4 % ($\times 49$ %)
Λ_C^+	2.9, 14	0.29, 1.4	≈ 60	$pK^-\pi^+$	5.0 %
				$p\bar{K}^0(K_S^0 \rightarrow \pi^+\pi^-)$	1.15 % ($\times 69.2$ %)
				$\Lambda\pi^+(\rightarrow p\pi^-)$	1.1 % ($\times 63.9$ %)
B	1.3, 6.2	0.2, 0.9	≈ 500	$J/\psi(\rightarrow e^+e^-) + X$	1.2 % ($\times 6$ %)
				$D^0(\rightarrow D^-\pi^+) + X$	60 % ($\times 3.8$ %)
				$e^+ + X$	10.9 %
B^+	0.6, 2.7	0.1, 0.4	≈ 500	$\bar{D}^0(\rightarrow K^+\pi^-\pi^+)\pi^+$	0.5 % ($\times 3.8$ %)
B^0	0.6, 2.7	0.1, 0.4	≈ 500	$D^{*-}(\rightarrow K^+\pi^-\pi^-)\pi^+$	0.3 % ($\times 2.6$ %)
Λ_B^0	0.1, 0.5	0.015, 0.07	≈ 400	$\Lambda_C^+(\rightarrow pK^-\pi^+) + e^- + X$	9.9 % ($\times 5$ %)
				$\Lambda_C^+(\rightarrow pK^-\pi^+) + \pi^-$	0.6 % ($\times 5$ %)

by using external event generators or virtual Monte-Carlo with its internal sub-detectors's information. The input of the reconstruction process can be steered to receive data from Monte-Carlo simulation (off-line) or real data of the experiment (on-line), as shown in Figure 2.4. The reconstruction output is the Event Summary Data (ESD) containing the reconstructed charged particle tracks and its identification information. This ESD will then be used for the data analysis process of finding heavy-flavors, low-mass di-electrons and hypernucleus which are the main topics in study of QGP explained above.

During the development in the upgrading of detectors for the next LHC Run 3 (<http://lhc-commissioning.web.cern.ch>), AliRoot is also used for the simulation data from the implemented geometries therein to estimate physics performances.

2.4.2 ALICE-FAIR on-line framework: ALFA

The ALICE computing framework for LHC Run 3 requires the on-line reconstruction for non-triggering system with high data throughput. The system for data exchange between the different platforms requires scalability and reliability. This requirement has commonality to the FairRoot framework used in FAIR experiments (Al-Turany et al., 2012).

The ALICE-FAIR (ALFA) framework is designed to provide the high throughput on-line data exchange between different computer platforms (Al-Turany et al., 2015). Its data transport layer is based on FairMQ, the ZeroMQ messaging protocol used to exchange data between nodes (Al-Turany et al., 2014). In this approach, an input-data will be divided into several fractional threads, as shown in Fig 2.5. Each thread will be process in parallel independently. Finally, the output-data is carried out with less time consuming, compared to the single-thread. The performances has been tested and shown good results on the Ethernet-based and the InfiniBand-based prototypes.

After the on-line data transportation was archived, the next step is the on-line reconstruction approach which will be explained in the following subsection.

2.4.3 ALICE on-line and off-line framework: O²

Improving the precise measurements of heavy flavor hadrons, low-momentum quarkonia and low-mass di-lepton require large statistics. For these

rare events, the obscure signal in the huge background, using only the trigger mode alone is inefficiency. Therefore, the continuous read-out facility shall be implemented especially for TPC which is the main contributor to the data capacity. In this concept, the data throughput from the detector is estimated to be greater than 1 TB/s for Pb-Pb events.

The O² is designed to reduce the data throughput during the data-flow by combining on-line and off-line systems(Adam et al., 2015). The on-line data exchange is based on ALFA framework. During data taking, the data will be reconstructed and compressed in several steps, synchronously and asynchronously, namely the on-line reconstruction. To archive this sequence, the on-line calibration also perform concurrently. Figure 2.6 shows the flow of RAW data from the detector will be processed synchronously. Then, the compressed data will be stored, together with its Compressed Time Frame (CTF) information. The asynchronous process reconstructs the CTF-tagged data, with the calibration, and produce the ESD files keeping into the storage. The Quality Assurance (QA) is also published.

The O² is in development state and will be ready to use in the next LHC Runs 3 and 4.

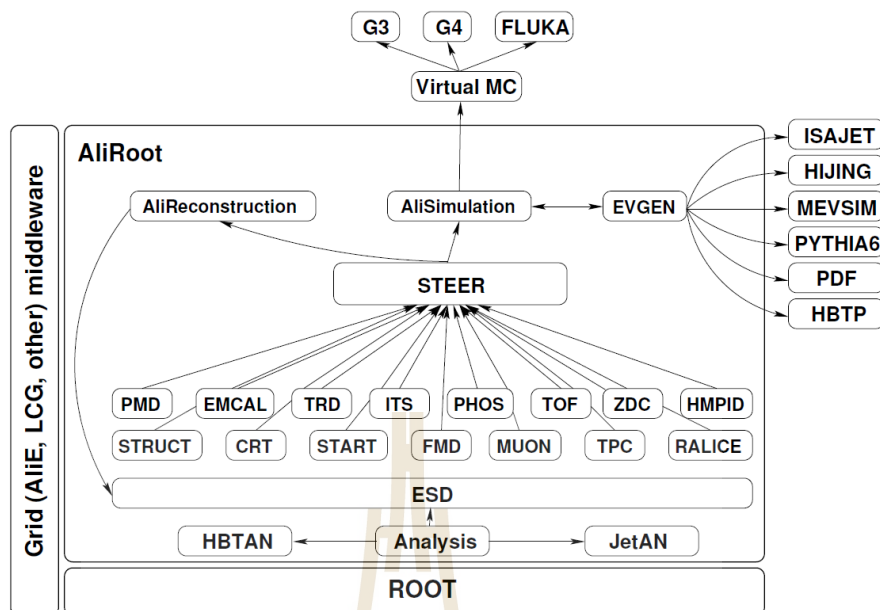


Figure 2.3 The schematic layout of the ALICE software framework: AliRoot. (Cortese et al., 2005)

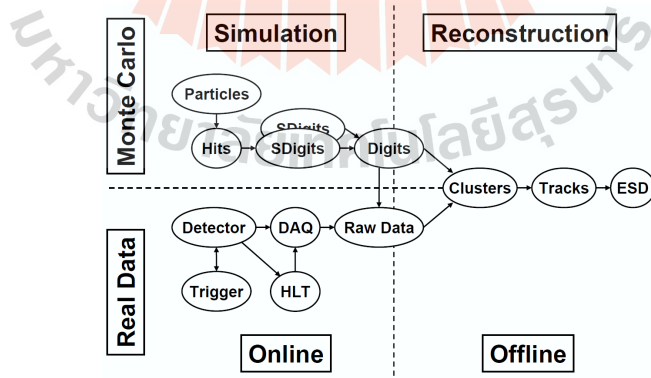


Figure 2.4 The organization of the on-line, simulation and reconstruction (off-line) processes. (Cortese et al., 2005)

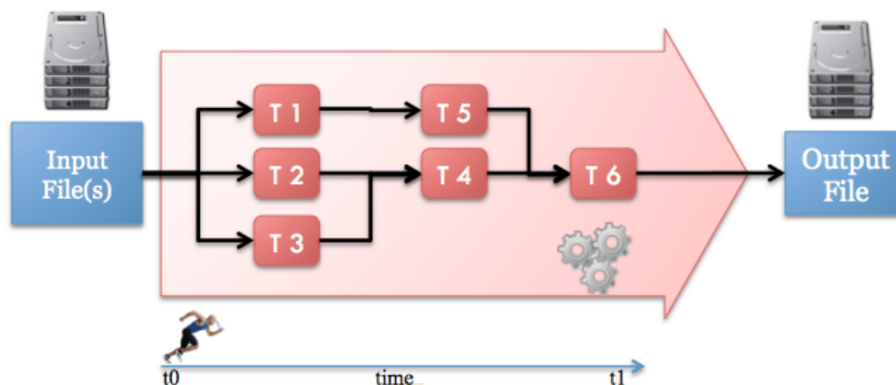


Figure 2.5 The organization of multiple threads run in parallel independently in ALFA nodes. (Al-Turany et al., 2014)

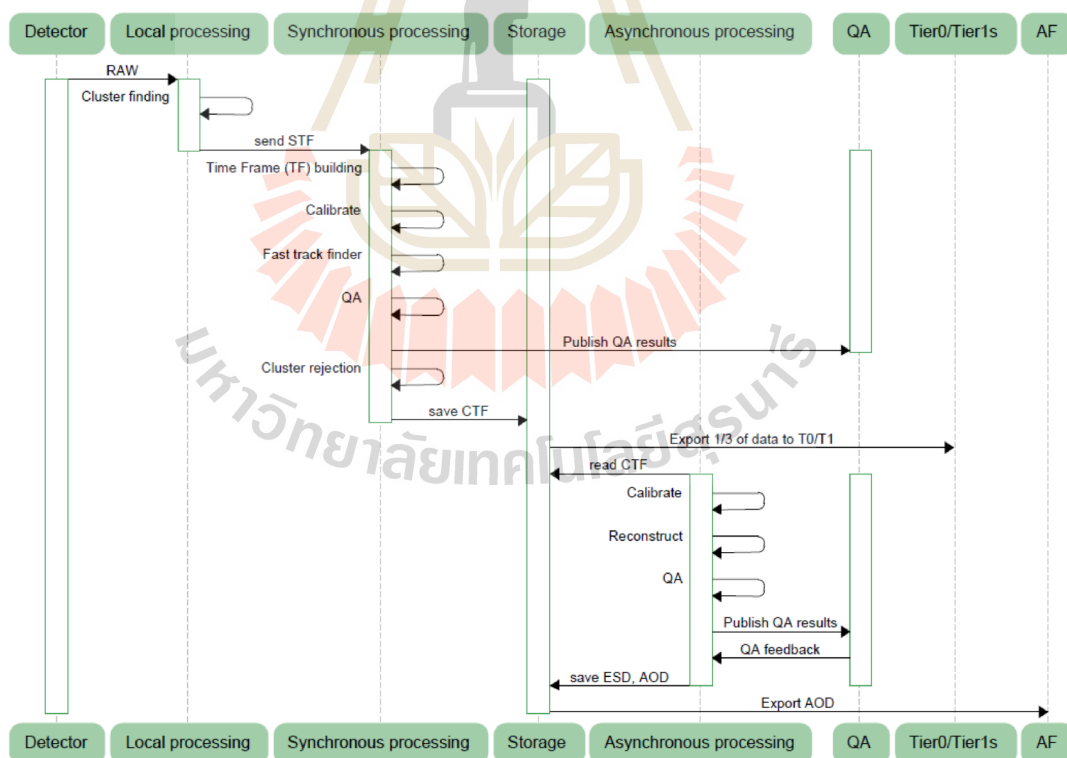


Figure 2.6 The data flow diagram for on-line reconstruction and calibration of the O². (Adam et al., 2015)

CHAPTER III

INTERACTION OF PARTICLES WITH MATTER

To detect particles, one need to know their interactions with detector mediums. Both charged and uncharged particles dissipate their energy while crossing through the material, by elastic and inelastic scattering processes mainly due to electromagnetic interaction. The energy loss for heavy particle come from ionization, while for β particle, the Bremsstrahlung is non-negligible. Another important process that significantly altered the detection ability presented in Table 2.1 is multiple Coulomb scattering (MCS).

In this chapter, we introduce the concept of material characteristic by the content of electron-energy-loss, namely the *radiation length* X_0 , in section 3.1. Then, section 3.2, a review of the energy loss by ionization in term of different materials. As followed, section 3.3 and 3.4 demonstrate additional energy losses by the Bremsstrahlung, pair production and electromagnetic cascade, in which X_0 is shown its contribution in those mathematical statements. Next, section 3.5, we consider the angle deflection by MCS which is the most important contribution concerned in PID approach. Finally, the commonly used parameter called the *material budget* X/X_0 is introduced in section 3.6.

Table 3.1 The values of L_{rad} and L'_{rad} for calculating the radiation length (Tsai, 1974).

Element	Z	L_{rad}	L'_{rad}
H	1	5.31	6.144
He	2	4.79	5.621
Li	3	4.74	5.805
Be	4	4.71	5.924
Others	> 4	$\ln(184.15 Z^{-1/3})$	$\ln(1194 Z^{-2/3})$

3.1 Radiation Length: X_0

The radiation length is usually measured in g cm^{-2} . It is the distance of traveled particle in which its energy decrease to a factor of $\frac{1}{e}$ in Bremsstrahlung process for high-energy electrons. It is also the $\frac{7}{9}$ of mean free path of pair production process for high-energy photons. The radiation length X_0 has been calculated by Y.S. Tsai (Tsai, 1974):

$$\frac{1}{X_0} = 4\alpha r_e^2 \frac{N_A}{A} \{Z^2 [L_{\text{rad}} - f(Z)] + ZL'_{\text{rad}}\}, \quad (3.1)$$

where Z is atomic number and A is mass number of the nucleus in material. L_{rad} and L'_{rad} are parameter involved the nuclear structure of target atom which are given in Table 3.1 for different materials. The function $f(Z)$ is calculated in H. Davies (Davies et al., 1954).

Dahl's private communication with PDG2006 (Yao et al., 2006) provides a simpler expression for an incident electron evaluated from a compact fit to the experimental data:

$$X_0 = \frac{716.4 A}{Z(Z+1) \ln(287/\sqrt{Z})} \text{ g cm}^{-2}. \quad (3.2)$$

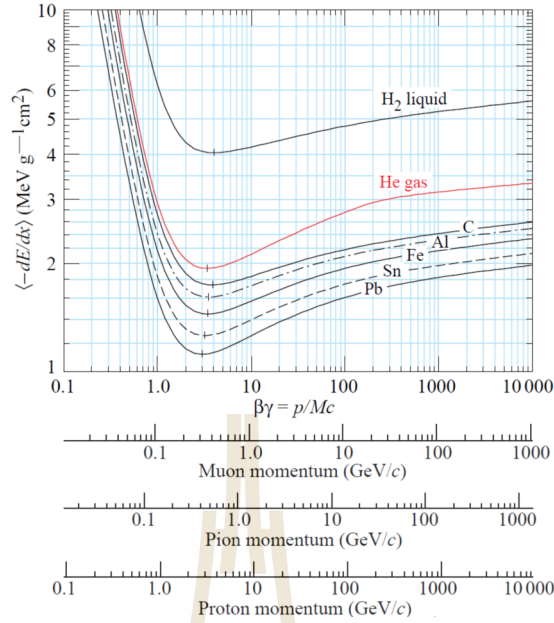


Figure 3.1 The examples of mean ionization loss rate in different material as a function of $\beta\gamma = p/Mc$ for muons, pions and protons, in bubble chamber. (Patrignani et al., 2016)

In case of compound material or mixture, the radiation length X_0 can be estimated by

$$\frac{1}{X_0} = \sum_i w_i \left(\frac{1}{X_0} \right)_i, \quad (3.3)$$

where w_i is weight fraction of substance i .

The list of radiation length for material with atomic number up to 92 was calculated by Tsai which shown in Table III.6 of (Tsai, 1974).

3.2 Energy Loss by Ionization

For intermediate-energy particles, the main contribution to energy loss for charged heavy particle by ionization can be described by the Bethe's equation

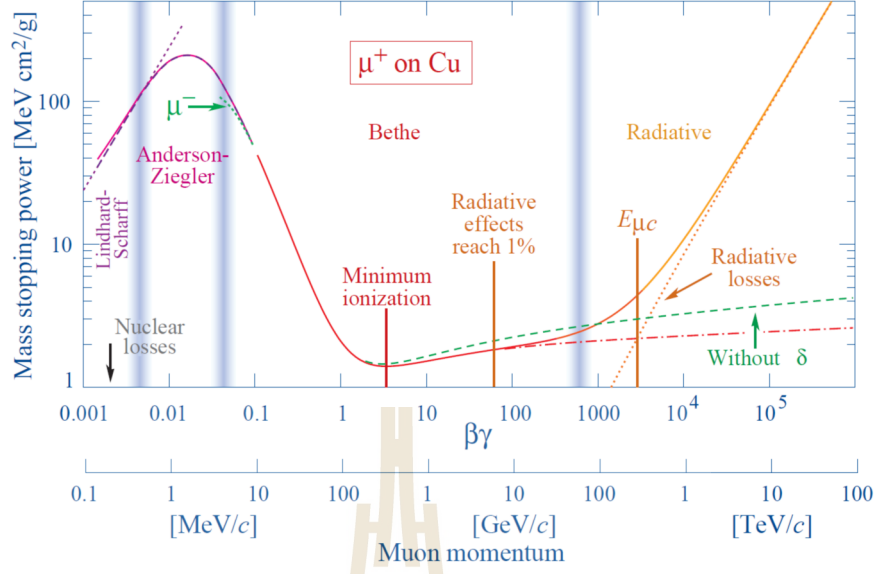


Figure 3.2 The mass stopping power for positive muons in copper against $\beta\gamma = p/Mc$. Solid curve is the total value. Vertical band is used for dividing the region of different approximation. The dotted line labeled “ μ^- ” is the Barkas effect for negative muons at low-energy of Bethe region. (Patrignani et al., 2016)

(Patrignani et al., 2016):

$$\left\langle -\frac{dE}{dx} \right\rangle = K z^2 \frac{Z}{A} \frac{1}{\beta^2} \left[\frac{1}{2} \ln \frac{2m_e c^2 \beta^2 \gamma^2 W_{\max}}{I^2} - \beta^2 - \frac{\delta(\beta\gamma)}{2} \right], \quad (3.4)$$

where A and Z are atomic mass and number of material, W_{\max} is the maximum energy transfer in a single collision, $K = 4\pi N_A r_e^2 m_e c^2 \approx 0.307075 \text{ MeV mol}^{-1} \text{ cm}^2$, γ is Lorentz factor and β is v/c . $\delta(\beta\gamma)$ is the density effect correction function which is usually using the Sternheimer’s parameterization (Sternheimer, 1952). This energy loss is called *mass stopping power*. Its unit is $\text{MeV g}^{-1} \text{ cm}^2$. The mean energy loss is slowly linearly decreasing with Z above the minimum value and also differed in different material, shown in Figure 3.1.

In case of low-energy particles, the Barkas correction has to be included (Barkas et al., 1956). It reduced the stopping power of negative particle to be

less than the positive one. This effect can be shown for muon interaction with copper in Figure 3.2. The Bloch correction is included in terms of high-order approximation in Equation 3.4. The shell correction is also included in order to correct some neglected contribution which the details are presented in (Ziegler, 1999).

3.3 Energy Loss by Bremsstrahlung and Pair Production

For high-energy charged particles, in addition to ionization process, an additional energy loss due to Bremsstrahlung in the Coulomb field of the atomic nuclei (Jackson, 1998). Bremsstrahlung is the process that de-accelerating charged particle radiate energy when deflected by another charged particle, which is the particle in nuclei of a material in our consideration. In this case, the atomic electron of the medium has been taken into account, called the *screening effect*, which reduced the total cross section as the radiation length is increased. The Bremsstrahlung spectrum can be approximated in Y.-S. Tsai (Tsai, 1974) and simplified with the definition of radiation length X_0 given in Equation 3.1, thus

$$\frac{d\sigma}{dk} = \frac{A}{X_0 N_A k} \left(\frac{4}{3} - \frac{4}{3}y + y^2 \right), \quad (3.5)$$

where σ is the interaction cross section, k is the incident particle energy, $y = k/E$ is the fraction of the electron's energy transferred to the radiated photon. After included the Landua-Pomeranchuk-Migdal effect, dielectric suppression, complete-screening and critical energy approximations (Patrignani et al., 2016), the energy loss for electrons in the matter can be expressed in a simple form.

$$-\frac{dE}{dx} \approx \frac{1}{X_0} E \quad (3.6)$$

Since X_0 is independent of E we can integrate it to get the energy loss $E(x)$ over a distance x .

$$E(x) = E_0 e^{-x/X_0} \quad (3.7)$$

The alternative way to get the Bremsstrahlung energy loss is provided in J.D. Jackson (Jackson, 1998).

For high-energy photon, in contribution to the photon cross section, the pair production cross section is dominated. The approximation obtained from Tsai (Tsai, 1974) can be expressed:

$$\frac{d\sigma}{dx} = \frac{A}{X_0 N_A} \left[1 - \frac{4}{3} x(1-x) \right], \quad (3.8)$$

where $x = E/k$ is fractional energy transfer to the pair-produced electron (or positron) and k is incident photon energy. After the symmetric treatment the high-energy limit for the total cross section σ .

$$\sigma = \frac{7}{9} \left(\frac{A}{X_0 N_A} \right) \quad (3.9)$$

At very high-energy, both Bremsstrahlung and pair production are affected by quantum mechanical interference. They also dependence with X_0 . In this case, the details are given in (Patrignani et al., 2016).

3.4 Energy Loss by Electromagnetic Cascade

On a thick absorber, the high-energy electron or photon produce the electromagnetic (EM) shower inside the medium. This EM cascade can be scaled as the radiation length. The longitudinal profile for a different type of particles is

described by the gamma distribution:

$$\frac{dE}{dt} = E_0 b \frac{(bt)^{a-1} e^{-bt}}{\Gamma(a)}, t = x/X_0, \quad (3.10)$$

where a and b are free parameters, and $\Gamma(a)$ is the gamma function fitted to the distribution. As an example of EGS4 simulation, shown in Figure 3.3, the correlation showed that the radiation length also affects the shape of this profile.

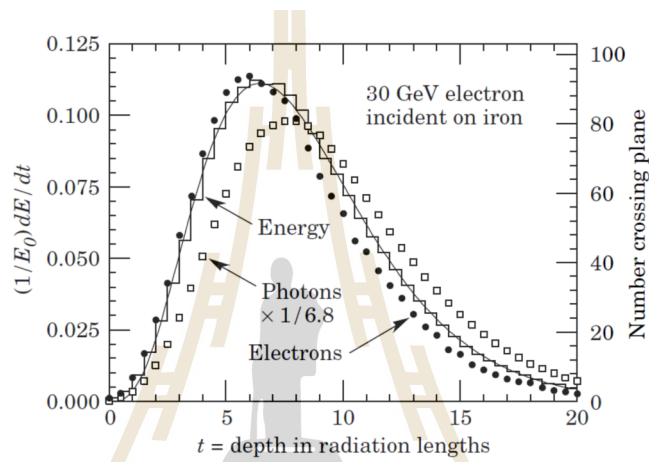


Figure 3.3 An EGS4 simulation of a 30 GeV electron-induced cascade in iron shown the differences between the shape of photons (square) and electrons (circle). The histogram shows fraction energy deposition per radiation length, and the curve is a gamma function fit to the distribution. (Patrignani et al., 2016)

It should be noted that this process is not considered in the ITSU SPD because of its thickness is in the order of micrometers.

3.5 Angle Deflection by Multiple Coulomb Scattering

A charged particle passing through the medium with thickness x will be deflected in many small angles, due to Coulomb interaction with nuclei. The net scattering (θ_{plane}) and displacement (y_{plane}) are Gaussian distribution. This multiple coulomb scattering (MCS) is well-represented by Molière theory (Bethe,

1953):

$$\theta_0 = \frac{13.6 \text{ MeV}}{\beta c p} z \sqrt{\frac{x}{X_0}} \left[1 + 0.038 \ln \frac{x}{X_0} \right] \quad (3.11)$$

where x/X_0 is the thickness of scattering medium in term of radiation length X_0 .

Figure 3.4 shown the layout to this effect which θ_{plane} is equal to θ_0 in equation

3.11. The parameter y_{plane} for Monte Carlo generation is expressed:

$$y_{\text{plane}} = \frac{1}{\sqrt{12}} z_1 x \theta_{\text{plane}} + \frac{1}{2} z_2 x \theta_{\text{plane}}, \quad (3.12)$$

where z_1 and z_2 are independent Gaussian random variables in the distribution.

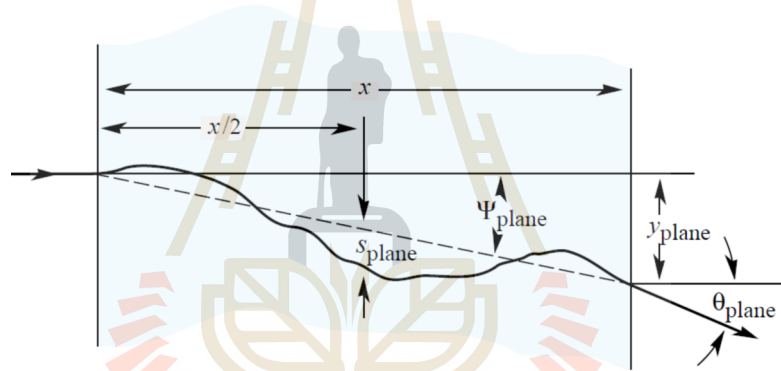


Figure 3.4 The layout of multiple Coulomb scattering shown the particle will be deflected in a small angle θ_{plane} in the plane of the figure. (Patrignani et al., 2016)

3.6 Material Budget: X/X_0

The X_0 contributed in equations 3.7, 3.10 and 3.11 are all represented in the form of X/X_0 . The physical meaning of this contribution is the thickness of scattering medium in term of radiation length X_0 , namely the *material budget*. It is also the fraction of the particle distance to its radiation length.

$$X/X_0 = \frac{\text{thickness}}{\text{radiation length}}. \quad (3.13)$$

In general, the contribution of material in percentage is more convenience to understand.

$$X/X_0(\%) = \frac{\text{thickness}}{\text{radiation length}} \times \text{surface } (\%), \quad (3.14)$$

where the percentage of surface indicated the unit amount of material used in the medium in gram percentage (g %).

For a single kind of material, the radiation length X_0 is given by equation 3.2 and the material budget is X/X_0 . In case of compound or mixture, the total material budget of all substances is the sum of each part,

$$\frac{X}{X_0} = \sum_n \left(\frac{X}{X_0} \right)_n, \quad (3.15)$$

where n is medium index in an region of calculation.

For example, the result shown in Table 3.2 is the material budget of the inner layer stave(Abelev et al., 2014b). It can give overall material budget of the stave but not in full details. To get the comprehensives result, we have to include the detailed geometry description into our calculation.

Table 3.2 List of estimated contributions of the inner layer stave to the material budget. Note that D is the thickness of the component. (Abelev et al., 2014a)

Stave element	Component	Material	D (μm)	X_0 (cm)	X_0 (%)
HIC	FPC Metal layers	Aluminium	50	8.896	0.056
	FPC Insulating layers	Polyimide	100	28.41	0.035
	Pixel Chip	Silicon	50	9.369	0.053
Cold Plate	Carbon fleece	Carbon fleece	40	106.80	0.004
	Carbon paper	Carbon paper	30	26.56	0.011
	Cooling tube wall	Polyimide	25	28.41	0.003
	Cooling fluid	Water		35.76	0.032
	Carbon plate	Carbon fibre	70	26.08	0.027
	Glue	Eccobond 45	100	44.37	0.023
	Space Frame	Carbon rowing			
Total					0.262

CHAPTER IV

DETECTOR GEOMETRY AND IMPLEMENTATION

4.1 Inner Tracking System (ITS)

The current Inner Tracking System (ITS) composes of six cylindrical layers of silicon detectors surround the beam pipe: the two innermost layers are Silicon Pixel Detectors (SPD), the two following layers are Silicon Drift Detectors (SDD) and the two outer layers are double-sided Silicon micro-Strip Detectors (SSD). The detector layout is shown in Figure 4.1. It covers the pseudorapidity range of $|\eta| < 0.9$ at the interaction point along the beam direction.

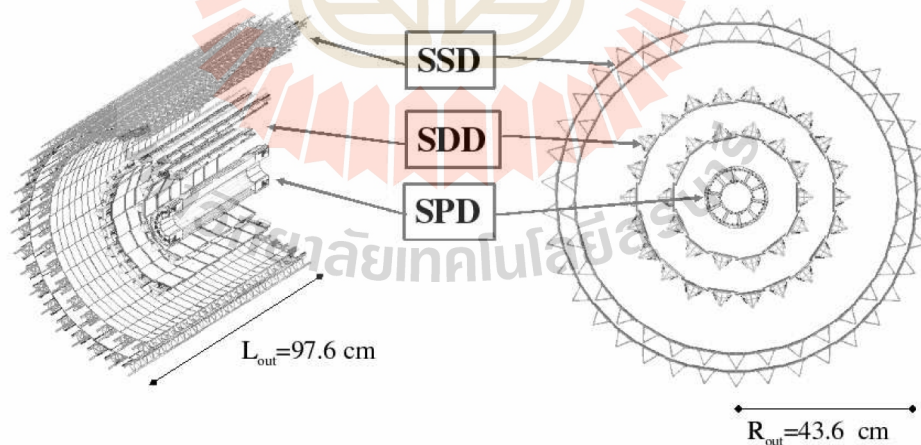


Figure 4.1 The ITS layout (Aamodt et al., 2008).

ITS is responsible for localizing the primary vertex with a high resolution, better than $100 \mu\text{m}$, detecting particles with momentum belows $200 \text{ Mev}/c$ and making the secondary vertex reconstruction from the decays of hyperons, D and

B mesons. The amount of material used in detector has been required to a minimum, to reduce the multiple scattering effects inside the detector medium which affect the momentum and impact parameter resolution for low-momentum particles. This amount is usually indicated by the percentage thickness in term of radiation length X_0 , namely the material budget.

4.2 ITS Upgrade (ITSU)

The new ITS detector structure have been proposed. It contains seven layers of SPD to improve tracking performance (Sitta, 2013). Each layer composes of several Staves (shown in Figure 4.2) circulating around the interaction point in the cylindrical form. It is divided into a tree inner layers (0-2), and four outer layers (3-6).

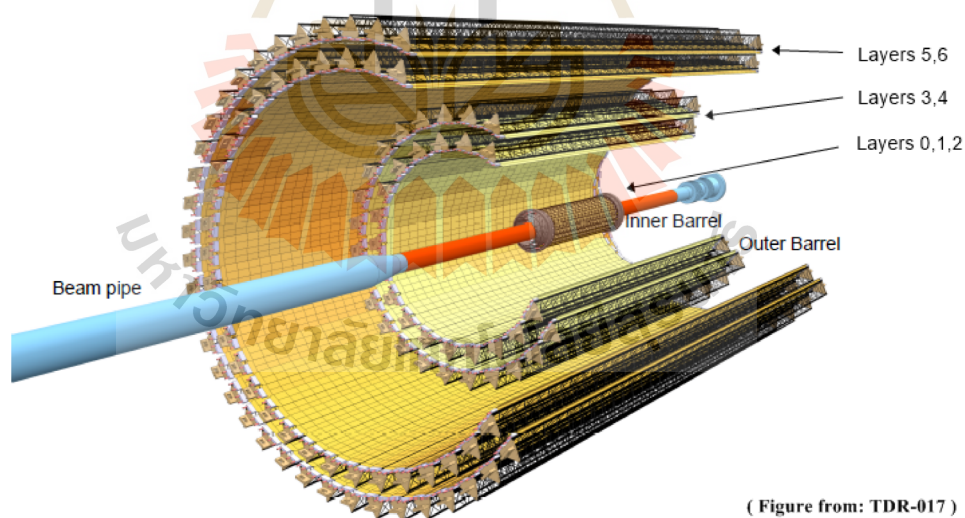


(Figure from: TDR-017)

Figure 4.2 ALICE ITS upgrade design layout (Musa, 2012).

The Inner Barrel (IB) and the Outer Barrel (OB), are designed for both service support and installation process (shown in Figure 4.3). Both are divided into two halves. Each barrel consists of Detector Barrel (DB) section and Service

Barrel (SB) section. The DB in each layer also has the structure used for support all Staves, called the End-Wheel. Each SB is the structure used for support all peripheral equipments including cables and cooling pipes.

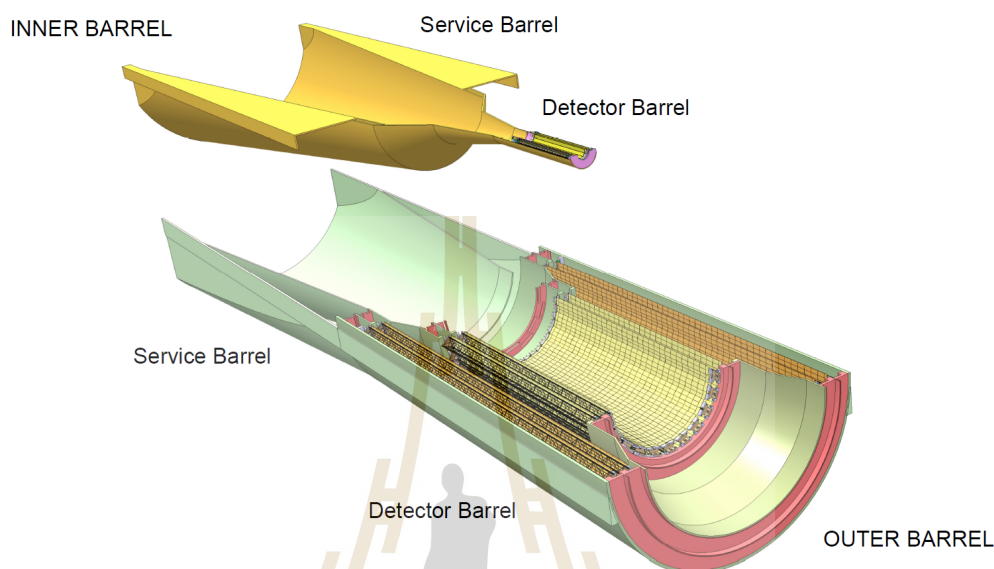


Figure 4.3 The layout of the new ITS barrels. Both Inner Barrel (IB) and Outer Barrel (OB). The visualization shown the half barrel for each types. (Aamodt et al., 2008)

Only IBDB is expected to be low material budget but not with the IBSB. During the development process one of the candidate models of IBSB has been proposed and the material budget is taken into account. The details will be explained in the next section.

4.3 ITSU with DC/DC Converter Unit (DCU)

The proposed IBSB includes the DC/DC Converter Unit (DCU) next to the Inner Barrel Detector Barrel (IBDB) Endwheels on A side (Figure 4.4). These DCUs have been designed to reduced the length of fluid pipes and power cables. Its location placed inside the sensitive area which could reduce the detector perfor-

mances of the secondary vertex detection (Belikov, 2014). In this case the material budget evaluation has been performed to estimate the possibility to use this model in the experiment.

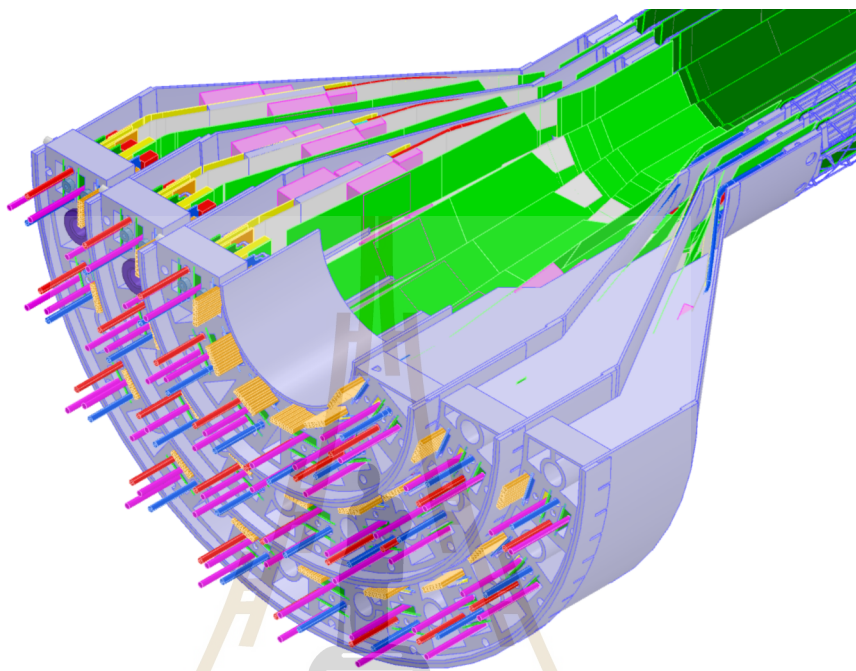


Figure 4.4 The IB layout of the new ITS candidate model with DCU. (Corrado, 3D(STP): 20151110_IB)

The trial IBSB design composes of three geometric carbon-fiber cones corresponding to the three ITS innermost layers. They are used for supporting the DCUs in detector layers. Each DCU connects one-to-one into each ITS Stave. It is composed of two DC/DC Converter Modules (DCM), hot and cold fluid pipes, heat exchange plate and the connector module shown in Figure 4.5. The FPGAs and some parts are disabled in this layout for visualization.

The DCM used for this model is the radiation and magnetic field tolerant 10W DC/DC converter module, FEASTMP_CLP. (<http://project-dcdc.web.cern.ch/>)

It is composed of several electronics parts which the radiation length cal-

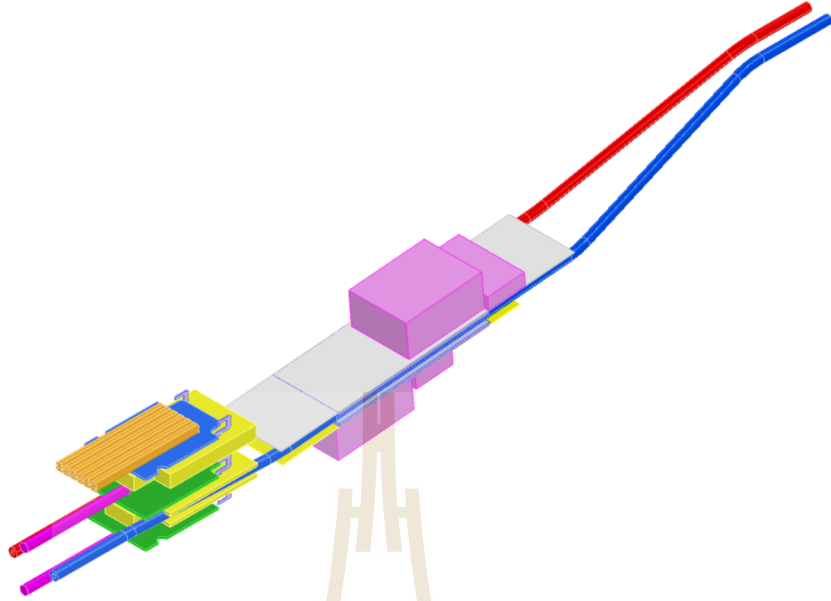


Figure 4.5 The DCU layout for each unit of ITS Stave. (Corrado, 3D(STP): 20151110_IB)

ulation could not be simplified. The material information used for input into the geometry through `AliROOT::AliModule` class is the function of either a material type i expressed in

$$Material_i = g(a_i, z_i, d_i, X_{0,i}, \lambda_i), \quad (4.1)$$

or a mixture type j of the materials $i = 1, \dots, N$ expressed in

$$Mixture_j = g(\{a_i, \dots, a_N\}_j, \{z_i, \dots, z_N\}, \{d_i, \dots, d_N\}_j, \{w_i, \dots, w_N\}_j), \quad (4.2)$$

where a is atomic mass, z is atomic number, d is density, X_0 is radiation length, λ is absorption length and w is concentration function, or weight fraction, expressed in

$$w_i = \frac{V_i}{V_f} = \frac{\text{Volume of a material } i}{\text{Volume of a mixture } j}, \quad (4.3)$$

and the material budget X/X_0 is the function of a contribution material length X . For simplicity, the combined material concept has been evaluated here.

4.3.1 Material Description

In this work the DCM object has been divided into three geometrical mixtures shown in Figure 4.6: PCB (grey plate), SHIELD (big pink box) and PASSIVE (small pink box). The material contribution to the DCM object are shown in Table A.1, Table A.2 and Table A.3 respectively.

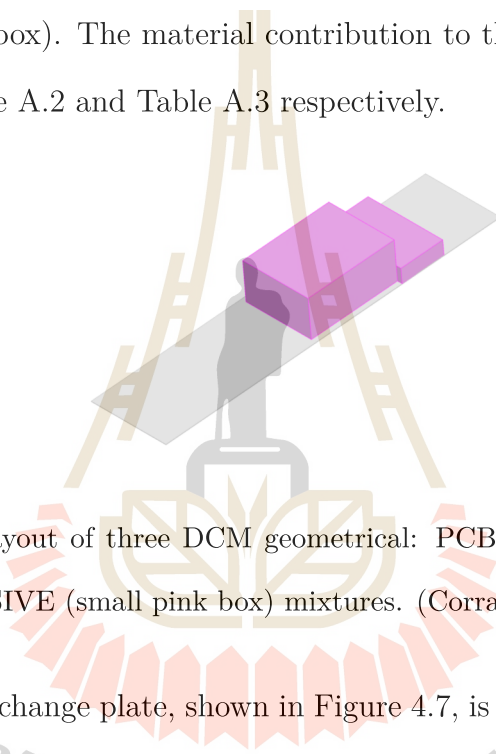


Figure 4.6 The layout of three DCM geometrical: PCB (grey plate), SHIELD (big pink box) and PASSIVE (small pink box) mixtures. (Corrado, 3D(STP): 20151110_IB)

The heat exchange plate, shown in Figure 4.7, is divided into two materials and one mixture: PLATE (grey plate) PIPE (blue pipe) and WATER (inside the pipes), respectively. Noted that the small part (light blue) is the connector which is the Polyurethane. This object uses the material information provided in AliRoot.

The DCU connectors, shown in Figure 4.8, also use provided material data given in AliRoot.

4.3.2 Implemented Geometry

The geometrical object results (Figure 4.10) were committed into AliRoot framework on 11/05/2015 with the corresponding class functions,

- for IBDB Endwheels and the support structure

```
AliITSUv2Layer::CreateInnerBEWheelA3(...)
```

- for all DCU arrays

```
AliITSUv2Layer::CreateInnerDCDCLayer3(...).
```

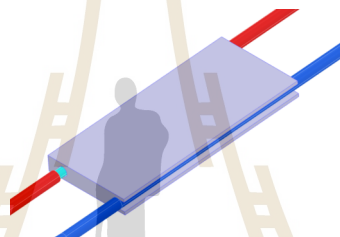


Figure 4.7 The layout of heat exchange plate and fluid pipes of a DCU. (Corrado, 3D(STP): 20151110_IB)

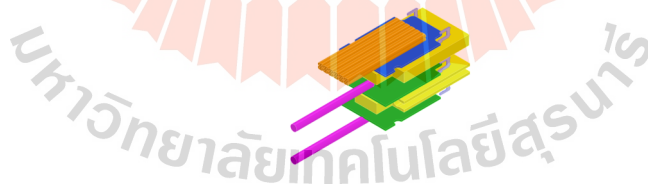


Figure 4.8 The layout of connectors at the tail of DCU. (Corrado, 3D(STP): 20151110_IB)

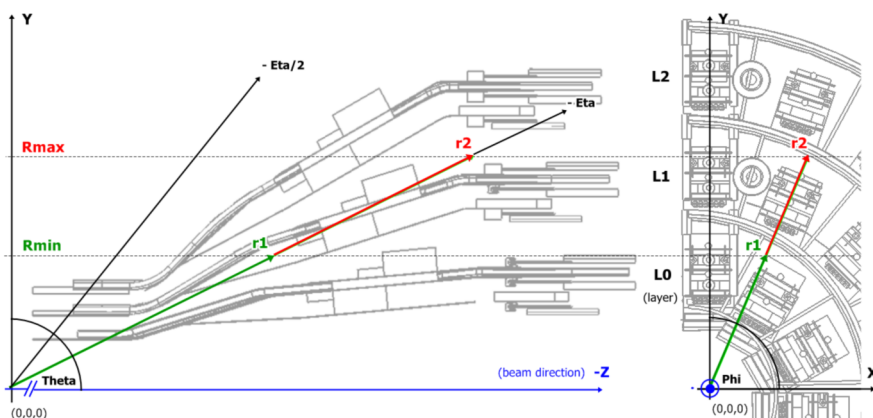


Figure 4.9 The layout of three layers of DCU in different detector coordinates.

(Corrado, 3D(STP): 20151110_IB)



Figure 4.10 The geometry of the ITSU IBSB with DCU which is already committed into AliRoot framework.

CHAPTER V

RESULT AND CONCLUSION

In order to calculate the material contribution, all material descriptions must be defined for all components in the geometry, described in section 4.3.1 of Chapter IV. Then we use the modified macros to produce the result histogram which will be described in the following sections.

To visualize the material budget in the complete histogram, the material descriptions are classified into six groups, called six scenarios, SHIELD, PASSIVE, PLATE, PIPE, COPPER and PCB. Each scenario is built in a sequential order, shown in Table 5.1. By running the macro, we generate one geometry file corresponding to the level number. All generated files will be used in the following section 5.1. This process is implemented in the macro files,

“AliRoot/ITSMFT/ITS/itsuTestBench/MaterialBudget/runMatBud.sh”.

5.1 X/X_0 Contribution

The material budget calculation process simulates the randomly particle tracks inside the geometry. Every material that a single track passing through is accounted and contributed into a fraction of material budget. The concept of scenario was provided to classify the material groups for visualization. The whole process is performed in a specific region which is considered to be a final result.

Table 5.1 The build level scenarios for material budget calculation.

Level	Scenarios	Geometry File
1	PCB	geometry_0.root
2	COPPER	geometry_1.root
3	PIPE	geometry_2.root
4	PLATE	geometry_3.root
5	PASSIVE	geometry_4.root
6	SHIELD	geometry_5.root

5.1.1 Contribution to a Track

A point in the rectangular coordinate system is $\vec{r} = (\hat{x}x, \hat{y}y, \hat{z}z)$. The mean material budget X/X_0 for a single track i from the position \vec{r}_1 to the position \vec{r}_2 can be expressed in a function,

$$(\overline{X/X_0})_i = f(\vec{r}_{1,i}, \vec{r}_{2,i}). \quad (5.1)$$

This internal function is implemented in

- “AliROOT::AliTracker::MeanMaterialBudget(...)”.

Note that the return value is normalized.

5.1.2 Contribution to a Scenario

The mean material budget X/X_0 in a scenario s can be expressed in:

$$(\overline{X/X_0})'_s = \left[\frac{100 \sum_{k=1}^{w_j} (\overline{X/X_0})_k}{w_j \sin \theta'} \right]_{j,s}, \quad (5.2)$$

where w_j is the number of tracks, or weight, in each histogram bin j . In this work we use 300 histogram bins and 10,000 test tracks. The $\frac{1}{w_j}$ is the normalizing factor

in the number of tracks and $\frac{1}{\sin \theta'}$ is the extraction factor at pseudorapidity equal to zero. The constant 100 is the percentage conversion. The subscript k is the label of tracks found in each bin. Note that the horizontal axis of the histogram is ϕ .

5.1.3 Contribution to a Region

The material budget X/X_0 in a track in equation 5.1 is extended for substituting the randomly position function:

$$\vec{r}_{m,k} = (\hat{x}R_m \cos \phi_k, \hat{y}R_m \sin \phi_k, \hat{z}R_m / \tan \theta_k), \quad (5.3)$$

where R_m is a position of the starting point or the end point, according to the subscript m , in the cylindrical coordinate, corresponds to either minimum and maximum values respectively. The random position function are expressed:

$$\phi_k = \phi' \text{ Random}(0, 1) \quad (5.4)$$

$$\eta_k = \eta' \text{ Random}(-1, 1) \quad (5.5)$$

$$\theta_k = 2 \arctan(e^{-\eta_k}), \quad (5.6)$$

where the unit of ϕ' is radian, η' is dimensionless and R_m is meter. We substitute the equation 5.3 and 5.1 into the equation 5.2. The collection of results in histogram would be:

$$\overline{(X/X_0)}'_s = \left[\frac{100 \sum_{k=1}^{w_j} f(\vec{r}_{m,k})}{w_j \sin \theta'} \right]_{j,s}, \quad (5.7)$$

where $\theta' = 2 \arctan(e^{-\eta'/2})$. This process has been implemented in a macro file, “/AliRoot/ITSMFT/ITS/itsTestBench/MaterialBudget/GetMaterialBudget.C”.

The physical meaning of R_{min} and R_{max} , corresponding to $m = 1$ and 2 respectively, are the minimum and maximum radii in which the test tracks have been generated.

The results of equation 5.7 are the histograms corresponding to each scenario. Then we combine all those onto one plot including the legend text, to describe the information relevant to the plot. Finally this plot is save into a picture file.

5.2 Calculation Processes

5.2.1 Earlier Processes with Stave

The previous material budget calculation (Abelev et al., 2014b) were developed for the ITSU stave. These processes are summarized in the following steps:

1. find the files in “/AliRoot/ITSMFT/ITS/itsTestBench/MaterialBudget/”
2. edit both files “AliITSUv2.cxx” and “AliITSUv2Layer.cxx”
3. compile and build the system via “aliBuild . . .”
4. do the calculation via “RunMatBud.sh”
5. draw the plot via “MakeMatBudPlot.C”
(the macro “GetMaterialBudget.C” has been called here)
6. visualize the result via “Material-details.pdf”.

The result of material contribution from stave L0 (1st layer) with azimuthal distribution $\phi = 0$ to 1 and pseudorapidity $\eta = 0$ is shown in Figure 5.1. Each color in the plot corresponds to the percent of materials used.

5.2.2 Modified Processes with DCU

The new geometries of ITSU IBDB with DCU have been implemented into the AliRoot. They are compatible with the other geometries completely. In details, they are no overlap and consistent with the AliRoot coding conventions. In order to calculate the material budget for the new parts, we have to place the new geometries outside the wrap volume of barrels to prevent the overlapping with its mother wrap volume. Then we move them along the beam direction until the center of DCU is in the same axis as the interaction point. The reason for this moving is to make sure that the new geometries cover the pseudorapidity range from -1 to 1 defined by our calculation processes. The parameters R_{min} and R_{max} for the DCU in L1 (2nd layer) are obtained from the measurement on 3D Computer Aid Design (CAD). The azimuthal distribution ϕ is in the range $0 - 90^\circ$.

The calculation processes and macros are also modified. We write two new macros, “MakeMatPlot.C” and “DrawMatPlot.C”. The script “RunMatPlot.sh” is also modified to call the macro “GetMaterialBudget.C” directly. In conclusion, the modified calculation processes are summarized in the following steps:

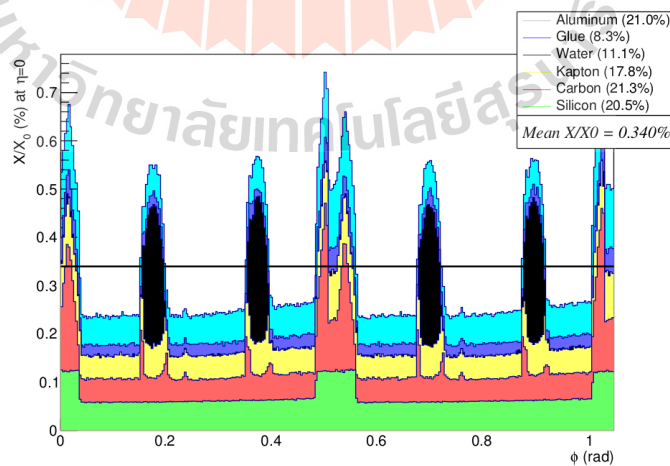


Figure 5.1 The result of material contribution of the ITSU stave L0 (first layer) is calculated from the earlier calculation processes. The horizontal line is the mean value.

1. edit both files “AliITSUv2.cxx” and “AliITSUv2Layer.cxx”
2. compile and build the system via “aliBuild ..”
3. do the calculation via the new macro “RunMatPlot.sh”
4. visualize the result via “Material-details.pdf”.

Then the result is shown in the Figure 5.2.

5.2.3 Consistency of The Modified Processes

The consistency of modified macros has been tested with the original geometries, the stave. All parameters were used the same as in the original processes. All geometries were enabled and moved back to the original position. We recalculate the material budget for stave L0 using the modified macros. The new result gives the same output as we calculate with the original macros. This confirms the consistency of modified macros used in this research.

5.3 Results

The material contribution to a DCU of the second layer (L1) is shown in Figure 5.2. The mean material budget is 1.392 % for azimuthal angle $\theta = 0 - 90^\circ$. The most material contribution of 69.4 % is heat exchange plate (PLATE) made of pure aluminum ($Z = 13$, $A = 27$, $X_0 = 24.01$). The PCB, PASSIVE, and SHIELD have contributions of 3.8 %, 3.5 % and 15.8 % respectively. In this work, the COPPER is pure copper and PIPE is Polyurethane (PE).

From our calculation, details are shown in the Figure 5.2, the mean material budget of DCU L1 is 1.392 %. It is almost two time higher than the design goals of the upgraded ITS (Sitta, 2013) for Outer Barrel Detector Barrel (OBDB), which

is only 0.8 %. In this case, the ability to detect low-momentum particles at the near edge of the OBDB will be reducing.

5.4 Conclusion

In this work, we have generated one of the candidate model for DC/DC Power Supply Unit (DCU) of the Inner Barrel Service Barrel (IBSB) of the ALICE Inner Tracking System Upgrade (ITSU). This model composes of DCU connected to the Inner Barrel Detector Barrel (IBDB) endwheels. These DCUs are located inside the sensitive region of the Outer Barrel Detector Barrel (OBDB) which could reduce the detection ability for low-momentum particles if there material budget values are higher than expected.

The implemented geometries have been committed to AliRoot framework at CERN. It has been confirmed that there is no overlap found. From our calculation the mean material budget of the DCU L1 is 1.392 %. The main contribution of 69.4 % comes from the heat exchange plate (PLATE) which is made of aluminum.

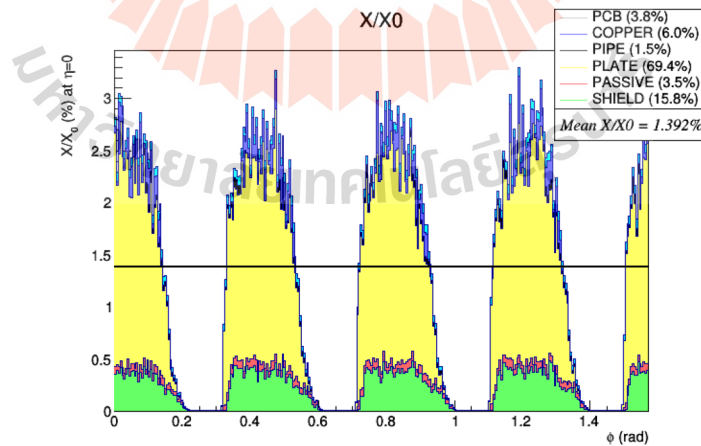
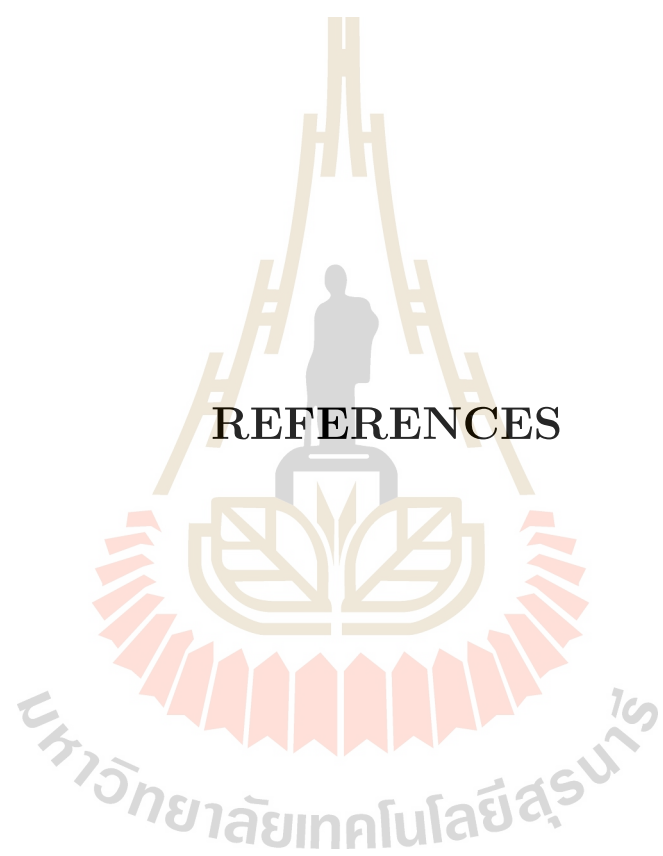


Figure 5.2 The material contribution of the ITSU IBSB DCU L1 with $\phi = 0 - 90^\circ$ is calculated from the modified calculation processes. The horizontal line is the mean value.

The calculated mean material budget is almost two time higher than material budget of OBDB stave. As a result this candidate model has been dropped. If we would like to continue with this model we have to find an alternative way to decrease the thickness of the heat exchange plate (PLATE) or replace it with another substance which has significantly lower material budget.





REFERENCES

REFERENCES

- Aamodt, K., Quintana, A. A., Achenbach, R., Acounis, S., Adamová, D., Adler, C., Aggarwal, M., Agnese, F., Rinella, G. A., Ahammed, Z., Ahmad, A., Ahmad, N., Ahmad, S., Akindinov, A., Akishin, P., et al. (2008). The ALICE experiment at the CERN LHC. **Journal of Instrumentation**, 3(08): S08002.
- Abelev, B., Abramyan, A., Adam, J., Adamová, D., Aggarwal, M., Agnello, M., Agostinelli, A., Agrawal, N., Ahammed, Z., Ahmad, N., Masoodi, A. A., Ahmed, I., Ahn, S., Ahn, S., Aimo, I., et al. (2014a). Performance of the ALICE Experiment at the CERN LHC. **International Journal of Modern Physics A**, A29:1430044.
- Abelev, B., Adam, J., Adamov, D., Aggarwa, M., Rinella, G. A., Agnello, M., Agostinelli, A., Agrawal, N., Ahammed, Z., Ahmad, N., Masoodi, A. A., Ahmed, I., Ahn, S., Ahn, S., Aimo, I., et al. (2014b). Technical Design Report for the Upgrade of the ALICE Inner Tracking System. **Journal of Physics G: Nuclear and Particle Physics**, G41: 087002.
- Abelev, B., Adam, J., Adamová, D., Aggarwal, M. M., Aglieri Rinella, G., Agnello, M., Agostinelli, A., Agrawal, N., Ahammed, Z., Ahmad, N., Ahmad Masoodi, A., Ahmed, I., Ahn, S. U., Ahn, S. A., Aimo, I., et al. (2014c). Upgrade of the alice experiment: Letter of intent. **Journal of Physics G: Nuclear and Particle Physics**, 41(8): 087001.
- Adam, J., Adamová, D., Aggarwal, M., Rinella, G. A., Agnello, M., Agrawal, N., Ahammed, Z., Ahn, S., Aimo, I., Aiola, S., Ajaz, M., Akindinov, A.,

- Alam, S., Aleksandrov, D., Alessandro111, B., et al. (2015). Technical Design Report for the Upgrade of the Online-Offline Computing System. **CERN Document Server**, CERN-LHCC(2015-006).
- Al-Turany, M., Bertini, D., Karabowicz, R., Kresan, D., Malzacher, P., Stockmanns, T., and Uhlig, F. (2012). The fairroot framework. **Journal of Physics: Conference Series**, 396(2): 022001.
- Al-Turany, M., Buncic, P., Hristov, P., Kollegger, T., Kouzinopoulos, C., Lebedev, A., Lindenstruth, V., Manafov, A., Richter, M., Rybalchenko, A., Vyvre, P. V., and Winckler, N. (2015). Alfa: The new alice-fair software framework. **Journal of Physics: Conference Series**, 664(7): 072001.
- Al-Turany, M., Klein, D., Manafov, A., Rybalchenko, A., and Uhlig, F. (2014). Extending the fairroot framework to allow for simulation and reconstruction of free streaming data. **Journal of Physics: Conference Series**, 513(2): 022001.
- Alessandro, B., Antinori, F., Belikov, J. A., Blume, C., Dainese, A., Foka, P., Giubellino, P., Hippolyte, B., Kuhn, C., Mart'inez, G., Monteno, M., Morsch, A., Nayak, T. K., Nystrand, J., Noriega, M. L., et al. (2006). Alice: Physics performance report, volume ii. **Journal of Physics G: Nuclear and Particle Physics**, 32(10): 1295.
- Barkas, W. H., Birnbaum, W., and Smith, F. M. (1956). Mass-ratio method applied to the measurement of l -meson masses and the energy balance in pion decay. **Physical Review**, 101: 778–795.
- Belikov, I. (2011). K_s^0 and Λ production in Pb-Pb collisions with the ALICE

experiment. **Journal of Physics G: Nuclear and Particle Physics**, G38: 124078.

Belikov, I. (2014). Event reconstruction and particle identification in the alice experiment at the lhc. **EPJ Web of Conferences**, 70: 00029.

Bethe, H. A. (1953). Molière's theory of multiple scattering. **Physical Review**, 89: 1256–1266.

Cortese, P., Dellacasa, G., Ramello, L., Sitta, M., Ahmad, N., Ahmad, S., Ahmad, T., Bari, W., Irfan, M., Zafar, M., Belogianni, A., Christakoglou, P., Ganoti, P., Petridis, A., Roukoutakis, F., et al. (2004). Alice: Physics performance report, volume i. **Journal of Physics G: Nuclear and Particle Physics**, 30(11): 1517.

Cortese, P., Dellacasa, G., Ramello, L., Sitta, M., Ahmad, N., Ahmad, S., Ahmad, T., Bari, W., Irfan, M., Zafar, M., Belogianni, A., Ganoti, P., Petridis, A., Roukoutakis, F., Spyropoulou-Stassinaki, M., et al. (2005). ALICE computing: Technical Design Report. **CERN Document Server**, CERN-LHCC(2005-018).

Davies, H., Bethe, H. A., and Maximon, L. C. (1954). Theory of Bremsstrahlung and Pair Production. II. Integral Cross Section for Pair Production. **Physical Review**, 93: 788–795.

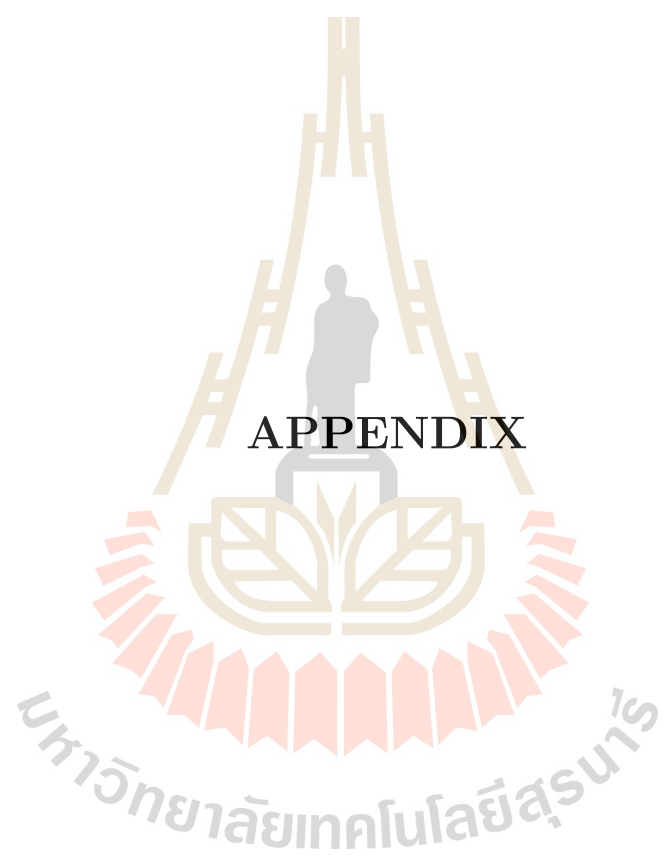
Fabjan, C. W., JirdÅln, L., Lindestruth, V., Riccati, L., Rorich, D., Van de Vyvre, P., Villalobos Baillie, O., and de Groot, H. (2004). ALICE trigger data-acquisition high-level trigger and control system: Technical Design Report.

- Jackson, J. D. (1998). Electromagnetic form factor corrections to collisional energy loss of pions and protons, and spin correction for muons. **Physical Review D**, 59: 017301.
- Mangano, M. L., Nason, P., and Ridolfi, G. (1992). Heavy quark correlations in hadron collisions at next-to-leading order. **Nuclear Physics B**, B373: 295–345.
- Musa, L. (2012). Conceptual Design Report for the Upgrade of the ALICE ITS. **CERN Document Server**, CERN-LHCC(2012-005).
- Patrignani, C., Agashe, K., Aielli, G., Amsler, C. and Antonelli, M., Asner, D., Baer, H., Banerjee, S., Barnett, R., Basaglia, T., Bauer, C., Beatty, J., Belousov, V., Beringer, J., Bethke, S., et al. (2016). Review of particle physics. **Chinese Physics C**, 40(10): 100001.
- Satz, H. (2011). The Quark-Gluon Plasma: A Short Introduction. **Nuclear Physics A**, A862-863: 4–12.
- Schukraft, J. (2012). Heavy Ion physics with the ALICE experiment at the CERN LHC. **Philosophical Transactions of the Royal Society A**, A370: 917–932.
- Sitta, M. (2013). The Upgrade of the ALICE Inner Tracking System. **Proceedings, 22nd International Workshop on Vertex Detectors (Vertex 2013)**, Vertex2013(02): 018.
- Sternheimer, R. M. (1952). The density effect for the ionization loss in various materials. **Physical Review**, 88: 851–859.
- Tsai, Y.-S. (1974). Pair production and bremsstrahlung of charged leptons. **Review of Modern Physics**, 46: 815–851.

Yao, W.-M., Amsler, C., Asner, D., Barnett, R., Beringer, J., Burchat, P., Carone, C., Caso, C., Dahl, O., D'Ambrosio, G., DeGouvea, A., Doser, M., Eidelman, S., Feng, J., Gherghetta, T., and others. (2006). Review of Particle Physics. **Journal of Physics G**, 33: 1+.

Ziegler, J. F. (1999). Comments on icru report no. 49: Stopping powers and ranges for protons and alpha particles. **Radiation Research**, 152(2): 219–222.





APPENDIX A

Table A.1 The material contribution of DCM PCB.

Part	Material(s)	Density	Weight fraction
Copper	Cu	9.86	0.090219864
FR4	Si	2.3296	0.15144894
	Ca	1.55	0.08147477
	Al	2.6989	0.04128158
	Mg	1.738	0.00904554
	B	2.08	0.0139757
	Ti	4.506	0.00287685
	Na	0.968	0.00445114
	K	0.862	0.00498089
	Fe	7.874	0.00209828
	F	1.696	0.0042
	O	0.001429	0.36043788
	C	2.1	0.27529426
	H	0.001251	0.01415852
N	0.00008988	0.03427566	

Table A.2 The material contribution of DCM SHIELD.

Part	Material(s)	Density	Weight fraction
Shield CU	Cu	9.86	0.011184966
Shield PE	C ₂ H ₄	0.96	0.187982625
Coil CU	Cu	9.86	0.013410143
Coil PE	C ₂ H ₄	0.96	0.094980695
SMD Inductor	Cu	9.86	0.000891892
Resistors	Al ₂	2.6989	0.000098852
	O ₃	0.001429	0.000087924
	Ni	8.908	0.000017375
	Sn	7.365	0.000013031
Capacitors	BaTiO ₃	6.02	0.016190646
	Ni	8.908	0.001506107
	Sn	7.365	0.001129580
AIR	CN ₂ O ₂ Ar ₂	0.00120479	0.672722674
Gap Pad	(GP300S30)	N/A	N/A

Table A.3 The material contribution of DCM PASSIVE.

Part	Material(s)	Density	Weight fraction
ASIC	Si	2.3296	0.005062500
SMD Inductor	Cu	9.86	0.007129630
Resistors	Al ₂	2.6989	0.000316083
	O ₃	0.001429	0.000281139
	Ni	8.908	0.000055556
	Sn	7.365	0.000041667
Capacitors	BaTiO ₃	6.02	0.051770089
	Ni	8.908	0.004815822
	Sn	7.365	0.003611867
Connector PE	C ₂ H ₄	0.96	0.059895833
Connector CU	Cu	9.86	0.023958333
AIR	CN ₂ O ₂ Ar ₂	0.00120479	0.843060638

CURRICULUM VITAE

NAME: Parinya Namwongsa **GENDER:** Male

NATIONALITY: Thai **DATE OF BIRTH:** September 11, 1980

EDUCATIONS:

- B. Sc. Department of Physics, Ramkhamheang University, Thailand, 2012.

PUBLICATIONS

- Namwongsa, P., Kobdaj, C. (2017). Material budget calculation of the inner DC-to-DC converters for ALICE Inner Tracking System upgrade. **The 7th International Graduate Research Conference, 19-20th Oct 2017, Ubon Ratchatani University, Thailand**, pp. 231-237.

[<http://www.nigrc2017.ubu.ac.th/igrc/index.php>]

- Namwongsa, P., Banjongkan, A., Chen, X., Giboni, K. L., Ji, X., Kobdaj, C., Yupeng, Y., and Kusano, H. (2017). Electron Recoil rejection by decay time measurement in large liquid Xenon detectors. **Journal of Instrumentation**, 12(04): P04019. [doi:10.1088/1748-0221/12/04/P04019]

- Namwongsa, P., Kobdaj, C. (2016). GEOMETRY DESCRIPTION OF THE ALICE INNER TRACKING SYSTEM UPGRADE. **Siam Physics Congress 2016, 8-10th Jun 2016, Ubon Ratchatani, Thailand**.

[<https://indico.cern.ch/event/478090/>]